Research Article | Vol. 29, No. 23 / 8 Nov 2021 / Optics Express 37733
Optics EXPRESS

Rapid prototyping of grating magneto-optical traps using a focused ion beam

XIAO SUN,[1,*] WILLIAM D. A. RICKARD,[1] BEN M. SPARKES,[2] BEN R. WHITE,[2] RACHEL F. OFFER,[2] ANDRE N. LUITEN,[3] AND CHARLIE N. IRONSIDE[1]

[1]John De Laeter Centre, Curtin University, Bentley, WA 6102, Australia
[2]Defence Science and Technology Group, Edinburgh, SA 5111, Australia
[3]Institute for Photonics and Advanced Sensing (IPAS) and School of Physical Sciences, University of Adelaide, 5005 SA, Australia
*xiao.sun@curtin.edu.au

Abstract: We have developed a rapid prototyping approach for creating custom grating magneto-optical traps using a dual-beam system combining a focused ion beam and a scanning electron microscope. With this approach we have created both one- and two-dimensional gratings of up to 400 µm × 400 µm in size with structure features down to 100 nm, periods of 620 nm, adjustable aspect ratios (ridge width : depth ~ 1 : 0.3 to 1 : 1.4) and sidewall angles up to 71°. The depth and period of these gratings make them suitable for holographic trapping and cooling of neutral ytterbium on the $^1S_0 \rightarrow {}^1P_1$ 399 nm transition. Optical testing of the gratings at this wavelength has demonstrated a total first order diffraction of 90% of the reflected light. This work therefore represents a fast, high resolution, programmable and maskless alternative to current photo and electron beam lithography-based procedures and provides a time efficient process for prototyping of small period, high aspect ratio grating magneto-optical traps and other high resolution structures.

1. Introduction

Magneto-optical traps (MOTs) are ubiquitous for the cooling and trapping of atoms [1] or molecules [2], and have resulted in the development of ultracold atomic systems with applications ranging from atomic clocks to quantum repeaters [3–5]. A disadvantage of using standard MOTs is the increased complexity of the physical system, as well as an increase in system size and a reduction in mechanical stability. Miniaturization of MOTs is therefore critical to create deployable cold-atom quantum devices able to operate in dynamic environments. To this end, various grating structures have been fabricated with photo or electron beam (e-beam) lithography techniques [6]. These grating MOTs (gMOTs) not only greatly decrease the optical complexity of an atom-cooling system, but also significantly reduce the device volume requirements and improve the reliability of the system. These devices are able to capture on the order of 10^8 atoms [6] and reach temperatures below 10 µK [7].

To date, commercial off-the-shelf diffraction gratings for creating a gMOT are only available for the relatively long trapping wavelength of Rubidium (Rb) atoms (780 nm) [8]. Recently, however, other atomic species such as ytterbium (Yb) have been shown to have desirable properties for the development of devices such as atomic clocks, as its electronic structure provides two optical transitions (399 nm and 556 nm) that can be used for laser manipulation, as well as a very narrow linewidth clock transition (578 nm) [9,10]. Due to this, Yb has also been touted as a possible candidate for a future revising of the definition of the second [11].

To be able to fabricate diffraction gratings for Yb, which has a trapping wavelength of 399 nm, requires a high-resolution fabrication process with grating period on the order of 500 nm. While modern electron-beam or photolithography processes are capable of creating such diffraction

#439479 https://doi.org/10.1364/OE.439479
Journal © 2021 Received 3 Aug 2021; revised 4 Oct 2021; accepted 20 Oct 2021; published 29 Oct 2021

Optics EXPRESS

gratings, for instance for trapping wavelengths of 671 nm [3] and 461 nm [12], these methods are inherently complex due to a series of necessary procedures including resist coating, exposure, development, etching and possible deposition and lift-off processes [13,14]. These treatments inevitably extend the production cycle, and introduce potential contaminations from the resist or metal layer. Furthermore, although sub-10 nm features can be achieved with the latest electron beam lithography (EBL) developments and high fidelity pattern transfer techniques [15,16], they usually incorporate a range of processes such as multiple lithographic patterning steps, sputtering and planarization, additional layers deposition or lift-off. These inevitably increase the fabrication complexity, require more facilities and have the potential to introduce different residual contaminations. Therefore EBL is more suitable for large size fabrication rather than fast prototyping of gratings. These issues have impeded the development of miniaturised MOTs for more exotic atom species such as Yb. In addition, the high number of processing steps of these methods increases the time for the iterative fabrication and test cycle, posing an increased challenge to rapid MOT prototyping.

Focused ion beam (FIB) fabrication, which employs a programmable ion beam sputtering routine (also referred as "rastering" or "milling" in some FIB fabrication work) combined with a high precision sample navigation system and advanced signal detectors, provides a multifunctional analytical platform for imaging, sputtering and nanofabrication [17]. Dual-beam FIB-scanning electron microscopes (SEMs) have a range of applications including cross-sectioning, three-dimensional reconstruction [18], site specific sample preparation for transmission electron microscopy (TEM) and atom probe tomography (APT) [19]. Modern FIB-SEMs can have ion beam spot sizes <10nm [20] and have advanced ion beam patterning capabilities which have opened up new opportunities in nanofabrication, for example the nanoscale machining of systems using programmable fabrication processes [17]. Material is sputtered away by the high energy primary ions (typically 30 keV Ga^+ ions) in a programmable area. The depth of the sputtered area and shape of the sidewalls is influenced by the sputtering routine, beam current and application time. Using a FIB-SEM integrated computer-aided design (CAD) systems, complex 3D structures can be fabricated [21–23]. Without traditional lithography and patterning procedures, FIB-SEM allows for maskless fabrication since it can directly write patterns on the specimen, significantly reducing fabrication complexity. Compared to conventional EBL-based fabrication method, the fabrication time of large structures is not an advantage of FIB-based methods. The FIB-based methods, however, can achieve design, patterning and SEM measurements in the same system, with an ion beam spot size below 10 nm [20]. In addition, no contamination such as resist residuals will be introduced in the process, which is critical to ensuring a clean surface for high performance gratings. A FIB-SEM system therefore provides a fabrication pathway that has sufficient resolution for rapid prototyping of diffraction gratings for compact cold-atom atomic clocks. Prior to this report, however, the required FIB fabrication conditions required for rapid prototyping have not been investigated before this report.

In this work we investigate the use of a FIB-SEM dual-beam system for rapid prototyping of diffraction gratings for cooling and trapping Yb atoms. This approach has the advantages of high precision positional beam control and complete automation for nanoscale patterning on a flat surface. It significantly simplifies the diffraction grating fabrication process for features down to 100 nm, fulfilling the requirements of small period and high aspect ratios for Yb trapping. Furthermore, the rapid design-fabrication-measurement cycle is conducted in just one or two facilities, providing a significantly reduced prototyping duration compared to conventional lithography-based procedures. The results from the fabrication and optical testing of various diffraction grating designs show that our technique is suitable for fast, programmable and maskless prototyping of grating structures.

Optics EXPRESS

2. Experimental methods

2.1. Design parameters

There are a number of interconnected parameters that must be considered when designing a diffraction grating for laser-cooling and trapping, to optimise the critical performance metrics of atom number and temperature. This includes minimising the amount of zero-order back-reflection, which can be achieved by fabricating a grating with depth [24]:

$$T = \frac{(2m-1)\lambda}{4}, \tag{1}$$

where m is an integer and λ is the wavelength of incident light. For Yb, with a trapping wavelength of 399 nm, this corresponds to a depth T=100 nm. Minimising the 0^{th} order back-reflection will also maximise the first order diffraction efficiency as, for a one-dimensional (1D) grating, assuming no higher-order diffraction or loss [25]:

$$2\eta_1 + \eta_0 = \rho, \tag{2}$$

where $\eta_{1(0)}$ is the $1^{st}(0^{th})$ order diffraction efficiency and ρ is the reflectivity of the medium. More generally, the 1^{st} order diffraction efficiency is given by [25]:

$$\eta_1 = \rho\frac{|1 + e^{i\pi[1-\frac{2T(1+\cos\alpha)}{\lambda}]}|^2}{8}, \tag{3}$$

where α is the angle of diffraction, determined by the period of the grating d:

$$\alpha = \sin^{-1}(\frac{\lambda}{d}). \tag{4}$$

Smaller diffraction angles lead to larger trapping volumes [26] but reduced damping and trapping coefficients [27]. In most cases, angles between 30° - 40° are used [3,6,27,28]. For Yb, the corresponding grating period is between 560 nm and 1 µm [23].

2.2. Fabrication methods

The substrates utilised in this work were 10 mm × 10 mm silicon (Si) wafer, diced from a 4-inch <100> p-type wafer, with a thickness of 460–530 µm and surface roughness of 2 nm. Nanofabrication of gratings was conducted using a Tescan Lyra3 FIB-SEM located at the John de Laeter Centre, Curtin University, which has a monoisotopic $^{69}Ga^+$ liquid metal ion source. This dual-beam system can achieve an imaging resolution of <2.5 nm (at 30 kV) for the Cobra FIB column, and 1 nm (at 30 kV) for the SEM column. The incorporated Python-compatible DrawBeam Advanced (TESCAN) software module was used for ion beam patterning. For this work, the ion beam energy was 30 keV, with a nominal scan rate of 0.295 μm^2/nA/s, dwell time of 1.0 µs and 0.1 spacing (90% overlapping of adjacent spots). Ion beam currents were varied from 35 pA to 600 pA. The FIB spot has a Gaussian shape [20] with a diameter dependent on the beam current, varying from 10 nm to 600 nm for the currents used in this study. A low beam current will produce a smaller beam diameter (high feature resolution), at the expense of a longer FIB fabrication duration.

Two FIB methods were employed for this work, as outlined in Fig. 1. Firstly, an FIB-only method utilised high density (typically 0.33 nC/μm^2) ions to sputter away Si directly to fabricate the grating structures (Fig. 1(a)). This method can be completed within the FIB-SEM dual-beam system, with imaging, sputtering and structure measurement being performed in the same facility in a convenient manner. In addition, a two-step nanopatterning method was used to write patterns with the FIB at relatively low ion density (typically <0.22 nC/μm^2) followed by removal of the

Optics EXPRESS

material with plasma etching (Fig. 1(b)). In this latter case, the FIB writing process implants Ga^+ ions into the sample surface where the implanted region forms a gallium oxide layer during plasma etching and serves as a hard mask for the etching [29,30]. A similar technique has been reported on diamond surfaces for high resolution fabrication [31]. Modelling through open source software SRIM indicated that the ion projected range (i.e., depth in the direction orthogonal to the sample surface) of Ga^+ in our silicon substrate is 27 nm with lateral straggling (i.e., in the direction parallel to the sample surface) of 7 nm, which are consistent with previously reported values [29]. Subsequently, samples were etched with an inductively coupled plasma reactive ion etching (ICP-RIE) system Plasmalab 100 (Oxford Instrument), using CF_4/O_2 plasma, an ICP power of 200 W, RF power of 100 W, at temperature of 20 °C. Dry etching of untreated Si is a relatively mature procedure, the plasma sources and ICP/RF powers were selected to accurately control the etch rate and depth based on our available RIE process capabilities. The corresponding grating depth was determined by the etching time (typically 79 seconds for 100 ± 5 nm).

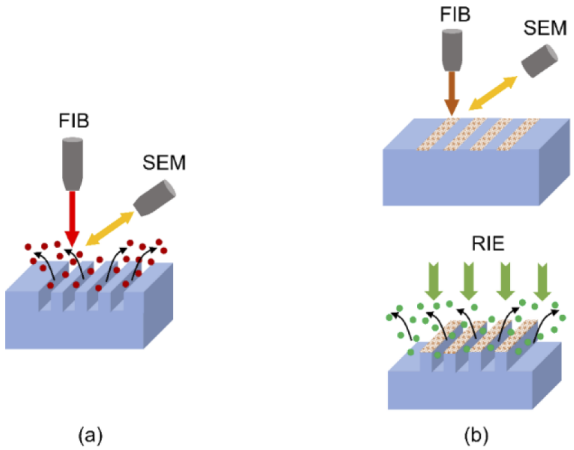

Fig. 1. Fabrication methods using focused ion beam (FIB). (a) FIB-only sputtering method, patterning by direct FIB sputter away materials; (b) FIB- reactive ion etching (RIE) combined method, FIB ion implantation with subsequent RIE to remove materials in un-implanted regions.

2.3. *FIB-SEM characterization of the gratings*

Cross-sections of the fabricated gratings are critical to investigate the structure parameters such as period, fill factor, sidewall angle and depth during prototyping. Although directly cutting structures with an ion beam is convenient for observation, it could introduce damage and deformation to the structured surface during sputtering. Furthermore, FIB sputtering alone produces a relatively low contrast image, which can be difficult to interpret. We instead used a platinum (Pt) protection layer-assisted technique to measure the gratings with high resolution SEM imaging, which was implemented in the same FIB-SEM chamber. Figure 2(a) shows the grating region to be investigated, followed by a ~200 nm thick Pt layer deposition with an electron beam on the region of interest in Fig. 2(b). This electron beam-assisted deposition avoids surface damage compared to deposition with an ion beam. Subsequently, an ion sputtering procedure was utilised to cut the Pt layer protected region. Finally, SEM imaging of the cross-section was performed with a −35° tilt correction applied to ensure measurements were accurate in the direction orthogonal to grating surface, to provide a high contrast cross-section view (Fig. 2(c)).

Optics EXPRESS

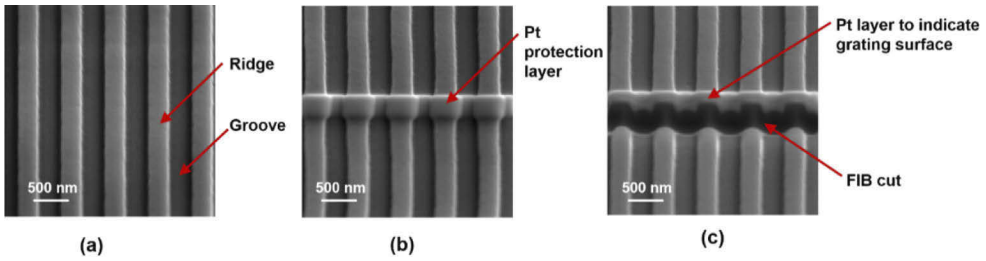

Fig. 2. Gratings fabricated and measurement techniques: (a) grating fabricated on silicon substrate; (b) Pt layer deposition to protect the grating; (c) after FIB cut of the Pt deposited region to observe the cross section.

2.4. *Optical characterization of the gratings*

Optical characterization of the gratings allows for direct measurement of the device performance in a non-invasive manner. These measurements, while lacking the resolution of the FIB-SEM method above, provide an average over the optical beam and can identify heterogeneity in the grating.

The set-up used for the optical testing is shown in Fig. 3, where the laser wavelength is 399 nm, corresponding to the neutral ytterbium $^1S_0 \rightarrow {}^1P_1$ 399 nm transition. Here, a translatable telescope system created an approximately collimated beam with a $1/e^2$ beam diameter of 130 µm at the grating, while moving the second lens allowed us to slightly focus the beam to a width of 100 µm for characterizing smaller gratings. By monitoring the optical power at positions A, B, and C we could measure η_0 and η_1, as well as the reflectivity of the substrate. These optically measured values, along with the measured angle of diffraction α, were used to determine the grating depth through solving Eq. (3) for T.

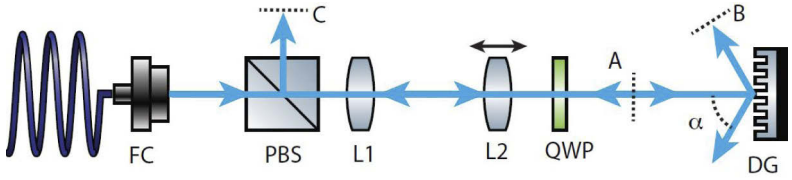

Fig. 3. Optical set-up to measure the performance of the fabricated gratings. FC – fibre coupler; PBS – polarising beam-splitter; L1, L2 – lenses which make up the translating telescope system; QWP – quarter wave-plate; and DG – diffraction grating. We measure the incident, and first and zeroth order diffracted powers at positions A, B and C, respectively, and α is the measured diffraction angle.

The polarization purity of the light diffracted from the grating is also an important parameter for creating a well-balanced atomic cloud with the lowest temperature possible. To determine the effect of the grating on polarization, a polarimeter was placed at location A to measure the polarization of the incident beam, and then at location B to measure the polarization after diffraction from the grating. For circularly polarized light, the purity of the polarization was determined through the degree of circular polarization (DOCP), which in turn can be calculated from the non-normalized Stokes parameters S_0, S_3 to be

$$DOCP = \sqrt{\frac{S_3^2}{S_0^2}}. \tag{5}$$

Optics EXPRESS

The measured DOCP of the incident light for both left and right circular polarizations was 98%.

3. Results

3.1. FIB-only fabrication

FIB-only fabrication parameters such as sputter routine, beam current and depth (aspect ratio) can influence the quality and speed of grating fabrication. To investigate these effects a series of gratings were produced and analysed.

3.1.1. Sputtering strategy

Beam patterning was investigated using two different sputtering strategies, as shown in Fig. 4. The fastest beam patterning routine involves moving the beam from one side of the sputter to the other in a single pass, however the disadvantage of this method is that some of the sputtered material remains in the patterned area, affecting the shape of the gratings. Minimal re-deposition was instead achieved when the beam was translated in a zig-zag pattern repeatedly over the area to be sputtered. Gratings fabricated with zig-zag and fast single scans are compared in Fig. 4(a), for a fixed ion beam current of 75 pA. We note from Fig. 4(a) that the zig-zag scan can fabricate a rectangular shape with a more uniform surface profile compared to a single scan sputtered pattern. For the single scan sputtered grating, the sputtering starting point (bottom of the image) and sidewall of the groove show re-deposition of the sputtered material, resulting in a significant deviation in the dimensions from the design parameters. Figure 4(b) and (c) further compare the cross section of gratings fabricated with the two strategies. Significant depth differences with zig-zag scanning (~100 nm) and fast single scanning (~460 nm) were measured. It can be seen in Fig. 4(c) that the re-deposition on the groove sidewalls also further reduces the groove width and increases the grating fill factor, which is undesirable for gMOT applications. Therefore the zig-zag scan sputtering strategy was employed in this work for directly writing patterns onto the sample.

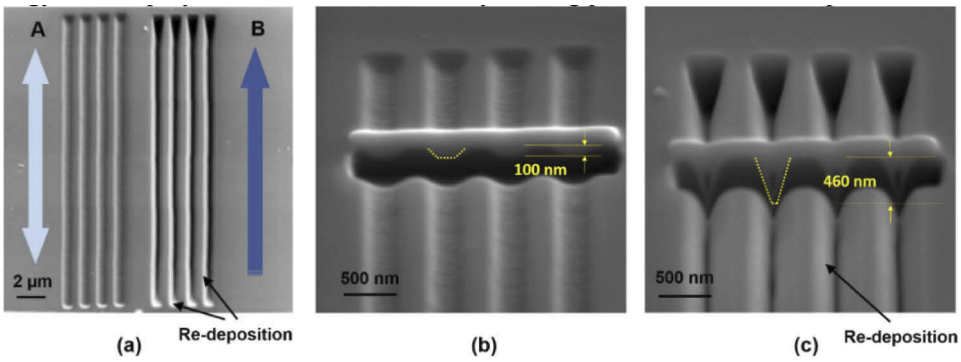

Fig. 4. Comparison of two sputtering strategies: (a) grating fabricated through A. zig-zag scan sputtering and B. fast single scan sputtering; (b) cross-section of zig-zag scan sputtered pattern; (c) cross-section of fast single scan sputtered pattern. Grating depth was measured with dotted lines to show the surface profile. An Ion beam current of 75 pA was used for sputtering in all cases.

3.1.2. Influence of the beam current

A comparison of gratings fabricated with a FIB energy of 30 keV and different ion beam currents is shown in Fig. 5, where the gratings were fabricated to have the same period and depth. As

Optics EXPRESS

expected, the reduction in beam current was directly linked to a reduced spot size and, as such, the sidewalls of the gratings were more vertical. This is observed for gratings fabricated with varied currents as shown in Fig. 5(a)-(d). However, when the FIB current was lower than 75 pA (Fig. 5(d)-(f)), the sidewall angle did not show a significant change, indicating a limit of fine structure fabrication was reached. Since the low current corresponds to a relatively long FIB sputtering time, a trade-off between fabrication duration and structure geometry needs to be considered. For instance, to create a 150 µm × 150 µm size grating the FIB sputtering duration is ~14 hours at 75 pA (Fig. 5(d)) or ~4 hours at 300 pA (Fig. 5(a)). In this work, to achieve relatively sharp sidewall angle and short FIB duration, the beam current for FIB-only method was set to 75 pA (~0.33 nC/µm^2).

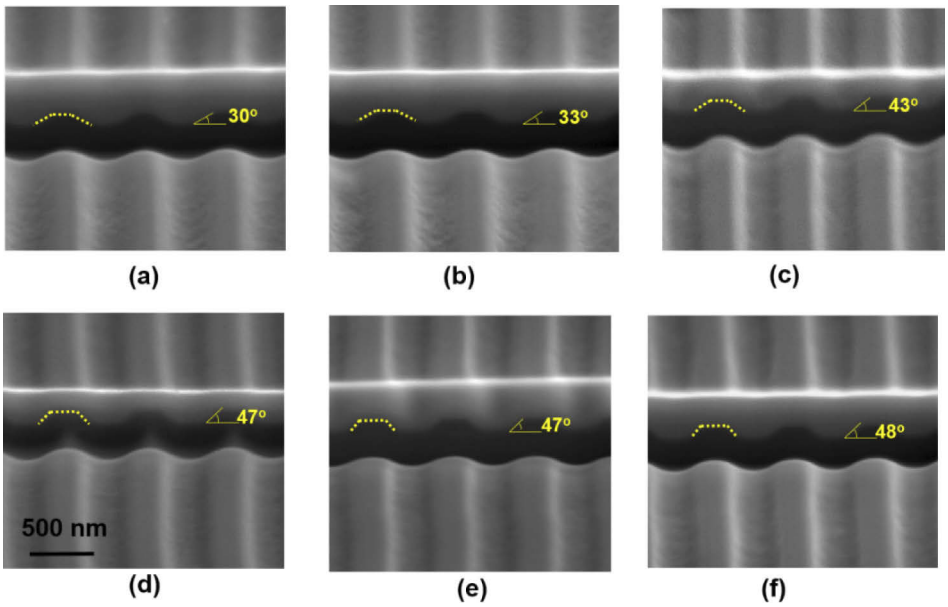

Fig. 5. Comparison of gratings fabricated with different ion beam currents. (a) 300 pA; (b) 200 pA; (c) 100 pA; (d) 75 pA; (e) 50 pA; (f) 35 pA. The sidewall angle (between the grating sidewall and the bottom) is included for each grating, with dotted lines showing the grating surface profile.

3.1.3. Control of the fill factor

The fill factor (i.e., the ratio of ridge width to grating period) plays an important role in the diffraction efficiency of a grating. Gratings fabricated with different fill factors are compared in Fig. 6, where the structures were designed to have the same period of 620 nm and a depth of 100 nm. A significant change in surface profile with the designed filled factor ranging from 60% to 30% can be seen in Fig. 6(a)-(d), with the corresponding ridge width dropping from 360 ± 10 nm to 180 ± 10 nm. Previous work on Rb gMOTs has found that optimal performance is achieved for a fill factor of 60% [25], which can easily be achieved through adjusting the sputtering width of rectangles in the FIB design program.

3.1.4. Control of the grating depth

The ability to fabricate high aspect ratio gratings is critical for achieving the required diffraction efficiency and angle for gMOT applications. The desired grating depth will be determined by the trapping wavelength of the particular atom, as demonstrated by Eq. (1). In Fig. 7 we compare the

Optics EXPRESS

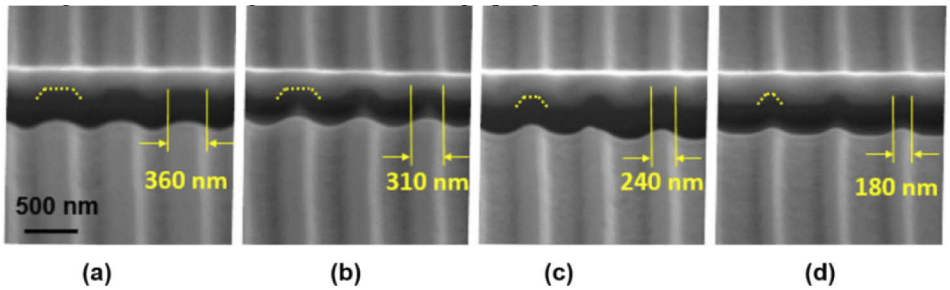

Fig. 6. Gratings fabricated with designed fill factor of (a) 60%; (b) 50%; (c) 40%; (d) 30%, which correspond to a design ridge width of 372, 310, 248, and 186 nm, respectively. The measured ridge width in each case is included in the figure, and dotted lines show the surface profile. An Ion beam current of 75 pA was used for sputtering in all cases.

fabrication of gratings with different depths achieved by varying the FIB sputtering time. In this case we have fixed the period to be 620 nm, the fill factor to be 50% and set the ion beam current to 75 pA. The depths of the gratings varied from 100 ± 10 nm to 420 ± 10 nm, resulting in aspect ratios (ridge width: depth) from 1 : 0.3 to 1 : 1.4. We varied the fabrication time rather than the ion beam current as it allowed for higher resolution features to be created, albeit at the expense of longer fabrication times.

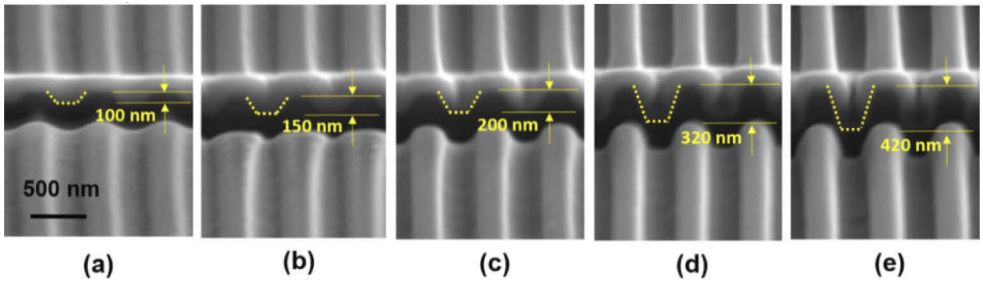

Fig. 7. Ion beam fabricated gratings with different aspect ratio: (a) 1: 0.3; (b) 1 : 0.5; (c) 1 : 0.6; (d) 1 : 1; (e) 1 : 1.4. Depth of grating is annotated respectively, with dotted lines to show the surface profile. An Ion beam current of 75 pA was used for sputtering in all cases, with different fabrication times used to achieve the various depths.

3.2. FIB and RIE combined fabrication

Gratings fabricated with the two-step FIB-RIE method are shown in Fig. 8, where two 400 µm × 400 µm gratings were fabricated on a 10 mm × 10 mm Si wafer (Fig. 8(a)). For each grating the ion implantation was implemented with FIB using a current of 400 pA for ~7 hours. Gratings were subsequently cut with a FIB to investigate the cross-sectional profile, as shown in Fig. 8(b)-(c). Accurate measurements of the grating profile were completed with the method described in Fig. 2, showing a sidewall angle of 71° for this sample. Compared to the best sidewall of ~48° for FIB-only method (Fig. 5), this FIB-RIE method has demonstrated significantly improved sidewall angle as well as surface flatness, which we find results in significantly enhanced optical performance.

Optics EXPRESS

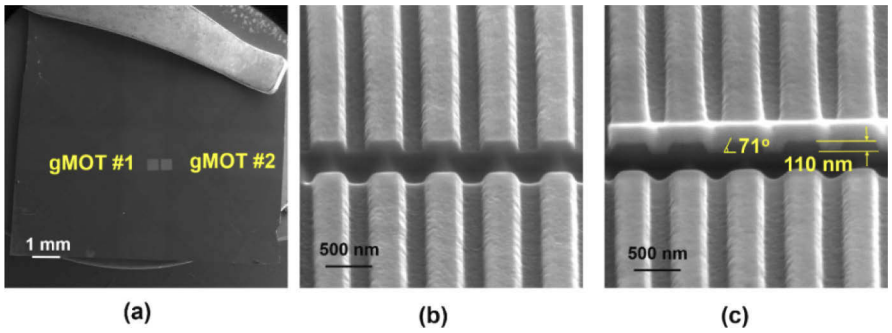

Fig. 8. SEM images of gratings fabricated with focused ion beam (FIB) and reactive ion etching (RIE), ion implantation was implemented with FIB at 400 pA. (a) Two gratings, each with an area of 400 µm × 400 µm; (b) FIB cut gratings to show the cross section; (c) platinum (Pt) layer deposition and FIB cut for accurate measurement of sidewall angle and depth of gratings (annotated).

3.3. gMOT pattern design

To trap atoms in three-dimensions, we need a two-dimensional (2D) grating pattern. The 2D geometries were designed through CAD software including Illustrator 2020 and KLayout 0.26.7, where the period and fill factor were programmable. Subsequently designs were exported to the FIB DrawBeam Advanced (TESCAN) for accurate ion implantation, followed by RIE processing.

We have designed and fabricated a tetrahedral (concentric triangular) grating, one of the simplest and most common types of gMOT geometries [3,6,28] for 399 nm light, as shown in Fig. 9(a). We have also created chess-board patterned gratings [6], which have a simple repeated geometry, shown in Fig. 9(b). However, the size of each of the gratings, which for fast prototyping were fabricated without stitching, was limited by the maximum view field (448 µm × 448 µm) of our FIB. This resulted in a tetrahedral grating with maximum side length of 300 µm and chess-board grating with a maximum size of 400 µm × 400 µm.

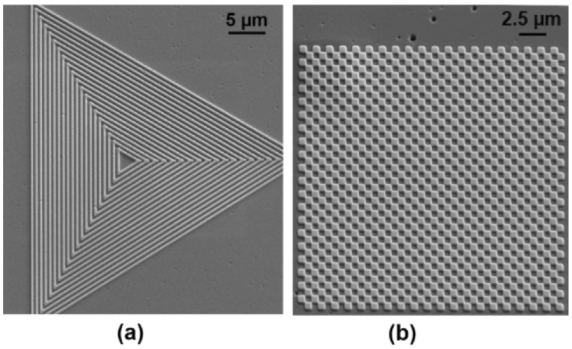

Fig. 9. Examples of different prototype diffraction grating patterns fabricated: (a) tetrahedral (concentric triangular) geometry with side-length of 40 µm; (b) chess-board (periodic squares) geometry of size 40 µm × 40 µm.

3.4. Optical measurements

Diffraction efficiencies of the 1D and 2D prototype gratings fabricated in this work have been measured to evaluate their optical performance. In this study the different gratings were designed

Optics EXPRESS

with a depth of ~100 nm (λ/4), a fill factor of 50% and a period of 620 nm, with corresponding aspect ratio (ridge width: depth) or 1: 0.3 and first order diffraction angle of 40°.

3.4.1. 1D gratings

Using the set-up shown in Fig. 3 and Eq. (2)–(4) we characterized the 1D gratings presented in Fig. 5(d) (FIB-only method) and Fig. 8(c) (FIB-RIE method). Table 1 shows the results obtained. For both methods of fabrication the depths deduced from the optical measurements were less than those measured with the SEM. This is most likely due to the non-ideal sidewall angles, which would explain why the difference is greater for the shallow sidewalls of the FIB-only method. To compensate for this, the design grating depth was adjusted to 110 nm, producing a total diffraction efficiency (i.e., combined η_{+1} and η_{-1}) of 40%. If the reflectivity of the wafer is taken into account, this corresponds to 90% of the reflected light being diffracted, demonstrating the benefit of a rapid prototyping and testing cycle. The DOCP for the FIB + RIE grating was measured to be 90% for both right- and left-circularly polarized incident light.

Table 1. Summary of SEM measurements, optical measurements and fitting for 1D gratings created using different fabrication techniques. NA: not applicable for a given measurement. SEM: measured from the SEM image; Optical: measured from the optical characterization (as a percentage of total incident power). * calculated via Eq. (4) from the SEM-measured grating period. ** calculated via (Eq. (3)) from the optical measurements of ρ, α, $\eta_{\pm 1}$.

Fabrication Technique	FIB		FIB + RIE	
Measurement	SEM	Optical	SEM	Optical
ρ (%)	NA	33	NA	43
α (°)	40*	38	40*	40
η_0 (%)	NA	11	NA	5
η_{+1} (%)	NA	13	NA	21
η_{-1} (%)	NA	11	NA	21
T (nm)	110	74**	110	91**

3.4.2. 2D gratings

Tetrahedral pattern – These gratings provide six diffracted beams. The average diffraction efficiency per beam, for the +1 and –1 orders, is given in Table 2. From fitting to the data we extract an effective optical depth of 78 nm, significantly lower than the 91 nm measured for 1D diffraction gratings. The large variation in efficiency from the three diffraction regions, captured by the standard deviation, is due to one of the three regions being significantly less efficient than the others. This could be due to the zig-zag FIB writing routine not following the direction of each of the triangle's sides, causing a reduction in the grating sidewall angle. A similar issue was also observed with the single scan sputtering strategy. A solution would be to rotate the sample and make the sputter routine parallel to each triangle side as it is being written. This will, however, require a much longer fabrication time due to the rotation of the stage and subsequent realignment procedures.

Chess-board pattern – These gratings provide two sets of diffraction patterns, one in the horizontal/vertical direction with a spacing determined by the period of the squares. A second pattern appears in the diagonal/anti-diagonal direction with a diffraction angle $\sqrt{2}$ smaller than the horizontal/vertical components. Diffraction into the diagonal/anti-diagonal pattern is significantly more efficient (totaling 30% of the incident light), and the average diffraction efficiency per beam for this pattern is given in Table 2. The total diffraction efficiency into the horizontal/vertical pattern represents 5% of the incident light. For this grating, we see a good fit with the 1D diffraction theory from Eq. (3) with a depth of 81 nm. The significant

Optics EXPRESS

Table 2. Summary of SEM measurements, optical measurements and fitting for different 2D grating structures. NA: not applicable for a given measurement. SEM: measured from the SEM image; Optical: measured from the optical characterization (as a percentage of total incident power) with η_1 being the average diffraction efficiency per beam, with the standard deviation shown in brackets. H/V: horizontal/vertical, D/AD: diagonal/anti-diagonal direction. * calculated via Eq. (4) from the SEM-measured grating period. ** calculated via Eq. (3) from the optical measurements of ρ, α, $\eta_{\pm1}$.

2D Pattern	Tetrahedral		Chess-Board	
Measurement	SEM	Optical	SEM	Optical
ρ (%)	NA	35	NA	42
α (°)	40*	43	H/V: 40*	H/V: 39
			D/AD: 27*	D/AD: 27
η_0 (%)	NA	8	NA	3
η_{+1} (%)	NA	4.8(3.5)	NA	7.8(0.8)
η_{-1} (%)	110	78**	110	81**

difference in efficiencies between diagonal/anti-diagonal and horizontal/vertical components agrees well with computer modelling [32]. To produce only one set of diffraction orders (i.e., the diagonal/anti-diagonal patterns) we will need to further reduce the grating period to less than 396 nm in the horizontal/direction, highlighting the need for high-aspect ratio fabrication. The DOCP for the diagonal/anti-diagonal diffracted beams was measured to be 97% for both right- and left-circularly polarized incident light.

4. Discussion

The FIB-only fabrication method uses just one system to complete the design, patterning, imaging and measurement, allowing accurate adjustment of the period, fill factor (aspect ratio) and depth with programmable FIB sputtering conditions in a convenient manner. However, this method requires relatively long FIB duration to complete the sputtering process. For example, with a beam current of 75 pA (Fig. 5(d)) for high resolution patterning, it would take ~133 hours to complete an area of 448 µm × 448 µm, which is the maximum single view field in our FIB. Long FIB sputtering durations will also be extremely challenging for the FIB system stability and grating repeatability. In addition, gratings fabricated with FIB-only method have relatively shallow sidewall angle of maximum 48° (Fig. 5).

In comparison, the two-step FIB-RIE method employs two systems to complete the fabrication process, the FIB duration was <10 hours for the same size of 448 µm × 448 µm, representing over a 10-fold speed-up in fabrication time. It also achieved a grating sidewall angle up to 71° (Fig. 8). It is obvious that shallower sidewall angles will impact the diffraction efficacy of the gratings, and a 90° sidewall angle is ideal for optical performance. This was also confirmed with our preliminary modelling and optical measurements of the 1D gratings. The sidewall angle can be affected by FIB spot size, redeposition (FIB-only method) and RIE parameters (FIB-RIE method). Close to 90 ° sidewall angles is possible through adapted etching techniques, such as cryostat deep RIE using liquid nitrogen assisted cryogenic etching [33]. However, the FIB-RIE method increases the complexity of the fabrication and has a potential to introduce contaminations in the plasma etching process. Therefore, the most appropriate fabrication method must be chosen depending on the application. The flexibility to easily alter the structure geometries without a mask allows for rapid investigation of the optimal parameters for a given regime, making the FIB based fabrication a desirable candidate for prototyping of diffraction gratings or other devices with a range of parameters to be studied in a quick test cycle.

For compact atomic clock applications, gMOTs are typically designed with an area of 20 mm × 20 mm [6,34]. To produce a sufficiently large number of trapped atoms it will be necessary to

Optics EXPRESS

scale our prototype gratings (which are 448 µm × 448 µm) up to larger areas (10–100 mm^2). The current maximum size of one grating is limited by the single view field of our FIB. Therefore we will need to implement high precision stitching of multiple gratings to produce the required size. This would be possible using an interferometric bench-based FIB, which can achieve stitching and juxtaposition of fields of the order of 20 nm over areas 100 mm ×100 mm in size [35]. The increased fabrication time for larger gratings must also be considered. As discussed previously, although the FIB + RIE method increases the fabrication complexity, the decreased FIB duration and sharp sidewall angle make this method preferable for large size grating fabrication. Another option would be to use conventional processes such as photolithography or EBL to create the larger grating once the design, fabrication and optical testing processes have been iterated sufficient times using the rapid FIB + RIE method.

Ideally, for the gMOT geometries investigated in this work, low 0th order diffraction efficiencies and high +1 order diffraction efficiencies are desired. This is required so that the diffracted beams create the necessary 3D radiation pressure to form a MOT, as well as balancing the downward force due to the incident beam in the direction perpendicular to the grating surface. For the 2D chess-board geometry (Fig. 9(b)), the 0th order diffraction was 3% and the total +1 order diffraction efficiency was 18%. This compares favorably with the tetrahedral (concentric triangular) geometry (Fig. 9(a)), where 9% 0th order diffraction was seen, as well as a significant drop in +1 order efficiency. In addition, when compared to the tetrahedral geometry, the chess-board geometry is much easier to accurately stitch due to its simple, repeated design. Therefore, in this work the 2D chess-board pattern is the most promising prototype grating fabricated at this stage for trapping Yb atoms in three dimensions.

However, before 2D gMOTs can be implemented in a cold-atom experiment, further investigation is required to increase the first order diffraction efficiency. For the 2D chess-board grating, although the total diffracted power is relatively high, this is currently spread over 8 beams due to diffraction from both diagonal/anti-diagonal and horizontal/vertical grating directions. Reducing the grating period so that diffraction is only possible from the diagonal/anti-diagonal grating should dramatically improve the diffraction efficiency per beam. The diffraction efficiency for the 1D geometries and 2D tetrahedral geometry could be improved by using blazed gratings, which have angled ridges, and should produce over 90% diffraction efficiency in the desired first order [36,37].

To improve the overall reflectivity, we have investigated coating the gratings with aluminium (Al) using physical deposition techniques [25] due to the greater than 90% reflectivity expected at 400 nm for Al film [38]. Initial testing using 100 ± 5 nm Al coatings via thermal evaporation has resulted in an increase in grating reflectivity up to 80%. However, further optical testing of these gratings has shown that the coating process results in a reduced grating depth. This highlights the need for a rapid prototyping process, as it allows for multiple fabrication, coating, and optical testing cycles to develop a grating with both the correct depth and high reflectivity to optimize the diffraction efficiency while minimizing zero-order reflections.

5. Conclusion

A FIB-SEM dual system was utilized for the fabrication of 620 nm period, 50% fill factor, high aspect ratio (ridge width: depth ~1:0.3) prototype diffraction gratings for laser-cooling and trapping of Yb atoms with a grating size of up to 400 µm × 400 µm. Factors affecting FIB-only fabricated gratings were investigated, with a range of profile parameters including sidewall angle, fill factor, depth and aspect ratio able to be controlled. A further investigation into a two-step method combining FIB ion implantation and plasma etching provided a promising approach to significantly improve the grating profile and reduce the FIB fabrication duration, while still being both maskless and high resolution. Different gMOT geometries were fabricated and tested in a manner that, when combined with optical testing, allowed for rapid prototyping to achieve

Optics EXPRESS

desirable properties for Yb atom trapping. Further improvements, including blazed grating, coating and scaling up the total area of the gMOTs through stitching multiple gratings together, will provide a path for the development of customizable diffraction gratings for applications including compact high accuracy atomic clocks and quantum repeaters.

Funding. Defence Science and Technology Group (QT71).

Acknowledgments. The authors acknowledge the support from John de Laeter Centre at Curtin University. The authors acknowledge the Western Australian node of the NCRIS-enabled Australian National Fabrication Facility (ANFF), and the support from the Western Australian Government's Department of Jobs, Tourism, Science and Innovation.

Disclosures. The authors declare no conflicts of interest.

Data availability. Data underlying the results presented in this paper are not publicly available at this time but may be obtained from the authors upon reasonable request.

References

1. E. Raab, M. Prentiss, A. Cable, S. Chu, and D. E. Pritchard, "Trapping of neutral sodium atoms with radiation pressure," Phys. Rev. Lett. **59**(23), 2631–2634 (1987).
2. A. L. Collopy, S. Ding, Y. Wu, I. A. Finneran, L. Anderegg, B. L. Augenbraun, J. M. Doyle, and J. Ye, "3d magneto-optical trap of yttrium monoxide," Phys. Rev. Lett. **121**(21), 213201 (2018).
3. D. Barker, E. Norrgard, N. Klimov, J. Fedchak, J. Scherschligt, and S. Eckel, "Single-beam zeeman slower and magneto-optical trap using a nanofabricated grating," Phys. Rev. Appl. **11**(6), 064023 (2019).
4. J. Rushton, M. Aldous, and M. Himsworth, "Contributed review: The feasibility of a fully miniaturized magneto-optical trap for portable ultracold quantum technology," Rev. Sci. Instrum. **85**(12), 121501 (2014).
5. P. D. Schwindt, Y.-Y. Jau, H. Partner, A. Casias, A. R. Wagner, M. Moorman, R. P. Manginell, J. R. Kellogg, and J. D. Prestage, "A highly miniaturized vacuum package for a trapped ion atomic clock," Rev. Sci. Instrum. **87**(5), 053112 (2016).
6. C. Nshii, M. Vangeleyn, J. P. Cotter, P. F. Griffin, E. Hinds, C. N. Ironside, P. See, A. Sinclair, E. Riis, and A. S. Arnold, "A surface-patterned chip as a strong source of ultracold atoms for quantum technologies," Nat. Nanotechnol. **8**(5), 321–324 (2013).
7. J. P. McGilligan, P. F. Griffin, R. Elvin, S. J. Ingleby, E. Riis, and A. S. Arnold, "Grating chips for quantum technologies," Sci. Rep. **7**(1), 384 (2017).
8. "Gmot-a compact grating magneto-optical trap chip for the generation of ultra-cold atoms," https://www.kntnano.com/quantum/gmotgrating/.
9. M. Schioppo, R. C. Brown, W. F. McGrew, N. Hinkley, R. J. Fasano, K. Beloy, T. H. Yoon, G. Milani, D. Nicolodi, and J. Sherman, "Ultrastable optical clock with two cold-atom ensembles," Nat. Photonics **11**(1), 48–52 (2017).
10. W. McGrew, X. Zhang, R. Fasano, S. Schäffer, K. Beloy, D. Nicolodi, R. Brown, N. Hinkley, G. Milani, and M. Schioppo, "Atomic clock performance enabling geodesy below the centimetre level," Nature **564**(7734), 87–90 (2018).
11. F. Riehle, P. Gill, F. Arias, and L. Robertsson, "The cipm list of recommended frequency standard values: Guidelines and procedures," Metrologia **55**(2), 188–200 (2018).
12. A. Sitaram, P. Elgee, G. K. Campbell, N. Klimov, S. Eckel, and D. Barker, "Confinement of an alkaline-earth element in a grating magneto-optical trap," Rev. Sci. Instrum. **91**(10), 103202 (2020).
13. X. Sun, A. Keating, and G. Parish, "Released micromachined beams utilizing laterally uniform porosity porous silicon," Nanoscale Res. Lett. **9**(1), 1–7 (2014).
14. J. Lee, G. Biedermann, J. Mudrick, E. A. Douglas, and Y.-Y. Jau, "Membrane mot: Trapping dense cold atoms in a sub-millimeter diameter hole of a microfabricated membrane device," arXiv preprint arXiv:2011.06692 (2020).
15. Y. Chen, Z. Shu, S. Zhang, P. Zeng, H. Liang, M. Zheng, and H. Duan, "Sub-10-nm fabrication: Methods and applications," Int. J. Extrem. Manuf. **3**, 032002 (2021).
16. Q. Liu, Y. Song, P. Zeng, C. Zhang, Y. Chen, H. Wang, Y. Luo, and H. Duan, "High-fidelity fabrication of plasmonic nanoholes array via ion-beam planarization for extraordinary transmission applications," Appl. Surf. Sci. **526**, 146690 (2020).
17. F. Niessen and M. J. Nancarrow, "Computer-aided manufacturing and focused ion beam technology enable machining of complex micro-and nano-structures," Nanotechnology **30**(43), 435301 (2019).
18. X. Sun, W. Rickard, C. Ironside, I. Kostakis, M. Missous, D. Powell, A. Anjomshoaa, and W. Meredith, "Targeted defect analysis in vcsel oxide windows using 3d slice and view," Semicond. Sci. Technol. **36**(6), 065015 (2021).
19. W. D. Rickard, S. M. Reddy, D. W. Saxey, D. Fougerouse, N. E. Timms, L. Daly, E. Peterman, A. J. Cavosie, and F. Jourdan, "Novel applications of fib-sem-based tof-sims in atom probe tomography workflows," Microsc. Microanal. **26**(4), 750–757 (2020).
20. P. Li, S. Chen, H. Dai, Z. Yang, Z. Chen, Y. Wang, Y. Chen, W. Peng, W. Shan, and H. Duan, "Recent advances in focused ion beam nanofabrication for nanostructures and devices: Fundamentals and applications," Nanoscale **13**(3), 1529–1565 (2021).

Optics EXPRESS

21. G. Lalev, S. Dimov, J. Kettle, F. Van Delft, and R. Minev, "Data preparation for focused ion beam machining of complex three-dimensional structures," Part B: Journal of Engineering Manufacture **222**(1), 67–76 (2008).
22. R. S. R. Ribeiro, P. Dahal, A. Guerreiro, P. A. S. Jorge, and J. Viegas, "Fabrication of fresnel plates on optical fibres by fib milling for optical trapping, manipulation and detection of single cells," Sci. Rep. **7**, 4485 (2017).
23. T. Loftus, J. Bochinski, and T. Mossberg, "Simultaneous multi-isotope trapping of ytterbium," Phys. Rev. A **63**(5), 053401 (2001).
24. J. P. Cotter, J. P. McGilligan, P. F. Griffin, I. M. Rabey, K. Docherty, E. Riis, A. S. Arnold, and E. A. Hinds, "Design and fabrication of diffractive atom chips for laser cooling and trapping," Appl. Phys. B **122**(6), 172 (2016).
25. J. P. McGilligan, P. F. Griffin, E. Riis, and A. S. Arnold, "Diffraction-grating characterization for cold-atom experiments," J. Opt. Soc. Am. B **33**(6), 1271–1277 (2016).
26. J. Franssen, T. de Raadt, M. van Ninhuijs, and O. Luiten, "Compact ultracold electron source based on a grating magneto-optical trap," Phys. Rev. Accel. Beams **22**(2), 023401 (2019).
27. J. P. McGilligan, P. F. Griffin, E. Riis, and A. S. Arnold, "Phase-space properties of magneto-optical traps utilising micro-fabricated gratings," Opt. Express **23**(7), 8948–8959 (2015).
28. R. Elvin, G. W. Hoth, M. Wright, B. Lewis, J. P. McGilligan, A. S. Arnold, P. F. Griffin, and E. Riis, "Cold-atom clock based on a diffractive optic," Opt. Express **27**(26), 38359–38366 (2019).
29. N. Chekurov, K. Grigoras, A. Peltonen, S. Franssila, and I. Tittonen, "The fabrication of silicon nanostructures by local gallium implantation and cryogenic deep reactive ion etching," Nanotechnology **20**(6), 065307 (2009).
30. I. Bobrinetskii, V. Nevolin, K. Tsarik, and A. Chudinov, "A distribution of ga+ ions in a silicon substrate for nano-dimensional masking," Russian Microelectronics **43**(1), 15–20 (2014).
31. S. K. Tripathi, D. Scanlan, N. O'Hara, A. Nadzeyka, S. Bauerdick, L. Peto, and G. L. Cross, "Resolution, masking capability and throughput for direct-write, ion implant mask patterning of diamond surfaces using ion beam lithography," J. Micromech. Microeng. **22**(5), 055005 (2012).
32. L. Li, "New formulation of the fourier modal method for crossed surface-relief gratings," J. Opt. Soc. Am. A **14**(10), 2758–2767 (1997).
33. H. V. Jansen, M. J. de Boer, S. Unnikrishnan, M. Louwerse, and M. C. Elwenspoek, "Black silicon method x: A review on high speed and selective plasma etching of silicon with profile control: An in-depth comparison between bosch and cryostat drie processes as a roadmap to next generation equipment," J. Micromech. Microeng. **19**(3), 033001 (2009).
34. E. Imhof, B. K. Stuhl, B. Kasch, B. Kroese, S. E. Olson, and M. B. Squires, "Two-dimensional grating magneto-optical trap," Phys. Rev. A **96**(3), 033636 (2017).
35. P. Mazarov, V. G. Dudnikov, and A. B. Tolstoguzov, "Electrohydrodynamic emitters of ion beams," Phys.-Usp. **63**(12), 1219–1255 (2020).
36. B. Schmidt, S. Wesch, T. Kövener, C. Behrens, E. Hass, S. Casalbuoni, and P. Schmüser, "Longitudinal bunch diagnostics using coherent transition radiation spectroscopy," arXiv preprint arXiv:1803.00608 (2018).
37. M. Vangeleyn, P. F. Griffin, E. Riis, and A. S. Arnold, "Laser cooling with a single laser beam and a planar diffractor," Opt. Lett. **35**(20), 3453–3455 (2010).
38. R. Hummel, "Reflectivity of silver-and aluminium-based alloys for solar reflectors," Solar Energy **27**(6), 449–455 (1981).